Letter

Primordial black holes, gravitational wave beats, and the nuclear equation of state

Thomas W. Baumgarte[1,*] and Stuart L. Shapiro[2,3,†]

[1]Department of Physics and Astronomy, Bowdoin College, Brunswick, Maine 04011, USA
[2]Department of Physics, University of Illinois at Urbana-Champaign, Urbana, Illinois 61801, USA
[3]Department of Astronomy and NCSA, University of Illinois at Urbana-Champaign, Urbana, Illinois 61801, USA

(Received 1 February 2024; revised 2 April 2024; accepted 13 June 2024; published 10 July 2024)

Primordial black holes (PBHs), if trapped in neutron stars, emit a characteristic continuous, quasiperiodic gravitational wave (GW) signal as they orbit inside the host star. We identify a specific and qualitatively new feature of these signals, namely quasiperiodic beats caused by the precession of noncircular PBH orbits. We demonstrate numerically and analytically that the beat frequency depends rather sensitively on the neutron star structure, so that hypothetical future observations with next-generation GW detectors could provide valuable constraints on the nuclear equation of state.

DOI: 10.1103/PhysRevD.110.L021303

Primordial black holes (PBHs), first proposed by [1,2], may have formed in the early Universe, and may contribute to or even make up most of its dark-matter content (see also [3]). While observational constraints on PBHs limit their possible contribution to the dark matter in some mass ranges, they remain viable candidates in other mass windows, including between about $10^{-16}M_\odot$ and $10^{-10}M_\odot$ as well as around $10^{-6}M_\odot$ (see, e.g., [4–6] for reviews and details).

If PBHs exist, some of them are likely to interact with stars and other celestial objects. Such interactions have been invoked as possible origins of several astrophysical phenomena, including the 1908 Tunguska event in Siberia [7] (but see [8]), neutron star (NS) implosions and "quiet supernovae" [9,10], fast radio bursts [9,11,12], the formation of low-mass stellar black holes [13–16], microquasars [17], and the origin of supermassive black holes (e.g., [18]), possibly via the formation of PBH clusters [19,20]. Gravitational-wave (GW) signatures of PBHs have been surveyed recently in [21], and the prospect of detecting PBHs using solar-system ephemerides has been discussed in [22,23] and references therein.

A collision with a star results in the PBH being gravitationally bound if it loses a sufficient amount of energy in the encounter, which is most likely to happen in collisions with NSs (see, e.g., [11,24–26]). The PBH may still emerge from the star, but can no longer escape to infinity. Losing more energy in subsequent passages, the PBH at some point remains completely inside the star, settles down toward its center, accretes stellar material, and ultimately induces the dynamical collapse of the host star (see [27–29] for numerical simulations). While the expected event rates are small (see, e.g., [24,25,30–32] as well as Sec. I in the Supplemental Material [33] for estimates) they depend strongly on a number of assumptions and may be more favorable in special environments, e.g., globular clusters and galactic centers. Small black holes may also form inside neutron stars from the collapse of other dark-matter particles (e.g., [10,27,34,35]), or be captured by neutron stars by other processes (e.g., [18,26,31,36]).

While the PBH spirals toward the center of the NS it emits gravitational radiation that—at least in principle—may be observable by next-generation GW detectors, and that would reveal information about the stellar structure [31]. The authors of [32,37], for example, examined this scenario assuming circular orbits. Since the PBH typically enters the host star on a noncircular orbit, and since the retarding forces inside the star may not circularize the orbit (see, e.g., [38,39]), the PBH's orbit is likely to remain eccentric (see also [40] for a numerical demonstration). In this Letter we discuss a qualitatively new feature of such noncircular orbits, namely continuous, *quasiperiodic GW beats*. These beats are caused by a precession of the PBH's orbit inside the star, the GW frequency for which is superimposed on the higher frequency arising from a single orbit. The resulting GW envelopes for the two GW polarizations are exactly out of phase, so that the GW signal alternates between being dominated by one or the other polarization. In the stellar interior, both Newtonian and relativistic effects contribute to this precession, but we find that the latter dominate in NSs. As we demonstrate both numerically and analytically, the rate of the precession, and hence the beat frequency, depends rather strongly on the NS structure, so that a future observation of such a GW beat

*Contact author: tbaumgar@bowdoin.edu
†Contact author: slshapir@illinois.edu

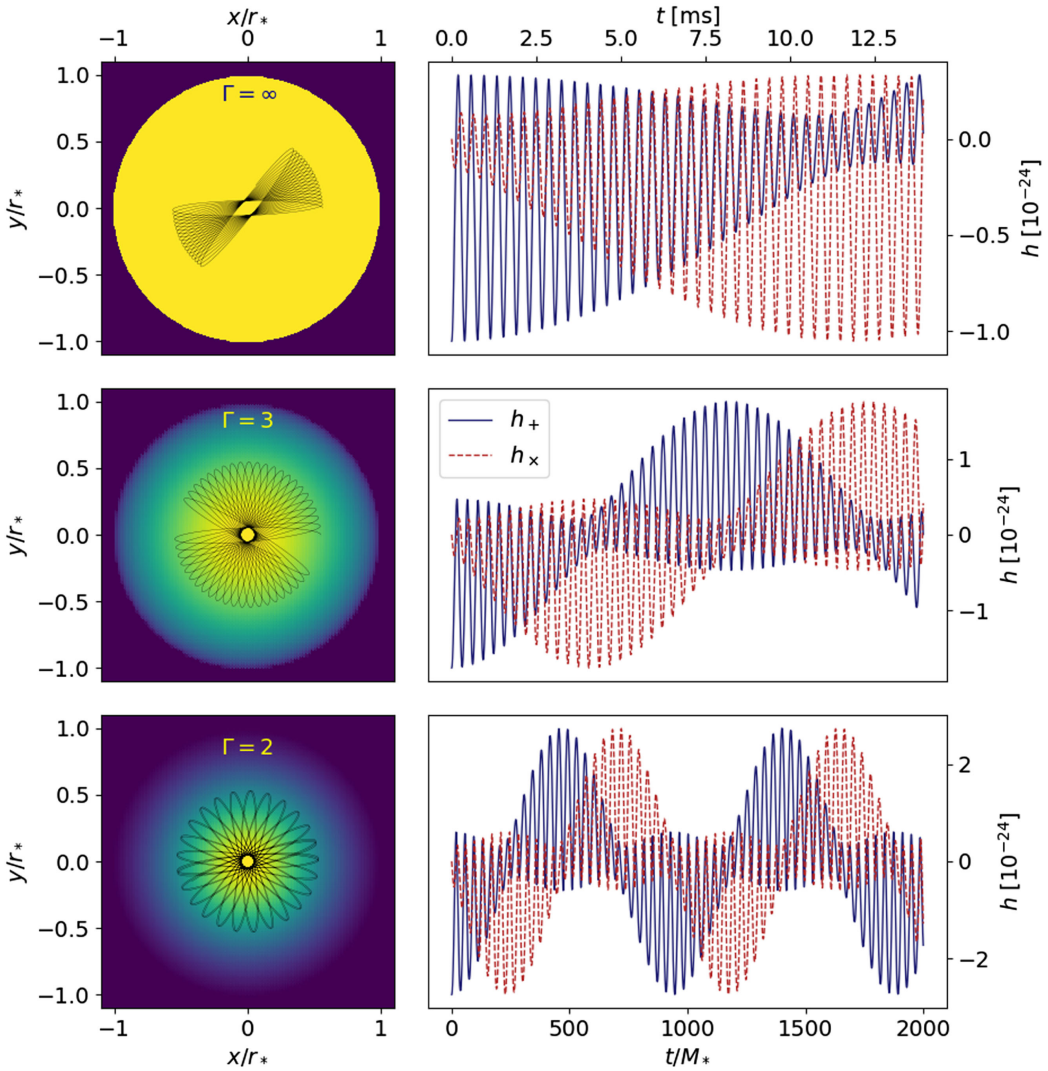

FIG. 1. Numerical examples of orbits inside NSs governed by different EOSs (left panels) together with the emitted GW signal as a function of time (right panels). The color shading in the left panels represents the density distribution inside the star. The top row shows, as the extreme limit, a constant-density star, corresponding to $\Gamma = \infty$. The middle and bottom rows show results for $\Gamma = 3$ and $\Gamma = 2$ polytropes. The GW amplitudes h_+ and $h_\times$ in the right panels are scaled for a star of mass $M_* = 1.4M_\odot$ and hosting a black hole of mass $m = 10^{-6}M_*$ at a distance of $d = 10$ kpc. The time t in the right panel denotes time as measured by a distant observer, and is provided both in units of the stellar mass M_* (bottom axis) and in terms of ms (upper axis). (See [41] for an animation.).

could provide strong constraints on the nuclear equation of state (EOS), let alone confirmation of the capture by a NS of a smaller and lower-mass intruder.

As a numerical demonstration we show in Fig. 1 characteristic orbits of PBHs inside NSs governed by three different EOSs varying in stiffness, together with their associated GW signals. We adopt a simple particle test-mass approximation to describe the PBH moving on geodesics in the gravitational field of a relativistic star. As dynamical friction and accretion drag forces are small perturbations that operate on secular timescales much longer than orbital times (e.g., [26,30]), we can probe the precession by neglecting these forces and examining a few orbits via geodesics. We assume the stars to be governed by a polytropic EOS

$$P = K\rho_0^\Gamma. \tag{1}$$

Here P is the pressure, ρ_0 the rest-mass density, K a constant, and the adiabatic exponent $\Gamma = 1 + 1/n$ may be expressed in terms of the polytropic index n. We construct the stellar models by solving the Oppenheimer-Volkoff (OV) equations, adjusting the central density so that the stellar compaction is always given by $GM_*/(c^2R_*) = 1/6$, where M_* is the star's total gravitational mass and R_* is areal radius (see Sec. II in the Supplemental Material [33] for details). In Fig. 1 we show examples for a star with constant total mass-energy density ρ (corresponding to

$\Gamma = \infty$), as well as $\Gamma = 3$ and $\Gamma = 2$ polytropes, which serve as examples of both highly and moderately stiff candidates for the NS EOS.

We then solve the relativistic geodesic equations in order to track the PBH's orbit. As discussed in Sec. III of the Supplemental Material [33], we choose to solve these equations in terms of the isotropic metric and radius r rather than the interior Schwarzschild metric and areal radius R, although the conversion is straightforward. We always start orbits with vanishing radial speed $u^r = 0$ at an initial (areal) radius $R(0) = R_{\rm frac}R_*$ and with angular momentum $\ell = \ell_{\rm frac}\ell_{\rm circ}$, where $\ell_{\rm circ}$ is the angular momentum corresponding to a circular orbit at radius $R(0)$. For the examples shown in Fig. 1 we used $R_{\rm frac} = 0.6$ and $\ell_{\rm frac} = 0.1$. All orbits are confined to a plane, which we arbitrarily take to be the $x-y$ plane. We also evaluate the leading-order GW signals h_+ and $h_\times$ along the z axis using the quadrupole formalism [42–44].

As can be seen in the left column of Fig. 1, the rate at which the PBH's orbit precesses depends strongly on the structure of the host star, and hence its EOS. For all three examples we show the orbits for a time span $\Delta t = 2000M_*$, which corresponds to about 14 ms for $M_* = 1.4M_\odot$. All orbits start out on the positive x axis. For the constant-density star in the top row, the orbit has rotated by just over 45° during this time, while for $\Gamma = 3$ it has rotated by a little less than 180°, and a little over 360° for $\Gamma = 2$.

If the GW signal is dominated by one polarization initially (in our case h_+), then it will be dominated by the other polarization after the orbit has rotated by 45°, and will return to the original polarization after a rotation through 90°. The resulting GW beats, and their dependence on the NS structure, can be seen in the right panels of Fig. 1. Specifically, we observe that the signal has shifted from being dominated by h_+ to being dominated by $h_\times$ for the constant density star, while for $\Gamma = 3$ it has gone from h_+ to $h_\times$ and then back to h_+ almost twice, and just over four times for $\Gamma = 2$.

The above behavior can be understood in part in the context of Bertrand's theorem ([45], see also [46]), which states that for potentials $V(R) = V_0 + kR^m$, where V_0 and k are constants, only the exponents $m = -1$ and $m = 2$ will always result in closed orbits.

The former exponent, $m = -1$, corresponds to a Newtonian point-mass potential, which is the leading order term in the potential in the exterior of a star. In general, deviations from this exterior potential result both from relativistic corrections as well as several Newtonian effects, including tidal and rotational deformations of the star (which are not present for our static spherical stars). These deviations result in precession of the orbit, including the well-known relativistic perihelion advance of Mercury (see Sec. IV.A of the Supplemental Material [33]).

The latter exponent, a harmonic-oscillator potential with $m = 2$, is realized in the interior of a Newtonian constant-density star, for which $M(R) = 4\pi\rho R^3/3$ and hence $V(R) = V_0 + 2\pi G\rho R^2/3$. In this case, deviations result from both density nonuniformities and relativistic corrections. While we do not expect any precession, either in the interior or exterior, for a homogeneous spherical star in Newtonian gravitation, relativistic effects will cause precession for such a star both in the exterior and interior.

Even for an inhomogeneous star, the stellar core becomes increasingly homogeneous as $R \to 0$. In Newtonian gravitation, the PBH's orbit therefore starts with a nearly closed orbit with $m = -1$ far outside the NS, and ends with a tighter, nearly closed orbit with $m = 2$ well inside the NS—quite remarkably realizing both cases of Bertrand's theorem as extreme limits. Moreover, since the approximately homogeneous core extends to larger radii for stiffer EOSs than for softer EOSs, we expect that, for a given orbital radius, the precession will be slower for a stiffer EOS than for a softer EOS in Newtonian theory. This precession rate variation is also found in general relativity, as revealed in the numerical examples of Fig. 1.

We can gain analytical insight into the above effects by considering small perturbations of circular orbits. Geodesics in static and spherically symmetric spacetimes possess two conserved constants of motion, namely the energy per unit mass $e = -u_t$ and the angular momentum per unit mass $\ell = u_\varphi$. Using the normalization of the four-velocity u^a, $g_{ab}u^a u^b = -1$, a first integral of the equations of motion can be written in the form

$$\frac{1}{2}(u^R)^2 = E - V_{\rm eff}(R), \tag{2}$$

where the constant $E \equiv (e^2 - 1)/2$ plays the role of the kinetic energy at infinity for velocities $v_\infty \ll 1$, and where we split the effective potential $V_{\rm eff}(R)$ into the two terms

$$V_{\rm eff}(R) = \frac{\ell^2}{2R^2} + V(R). \tag{3}$$

In many cases (e.g., a Newtonian point-mass) $V(R)$ is independent of e and l, but we now allow this term to depend on these two constants, which is the case for the orbits in general relativity considered here. In the following we assume the orbit to be in the equatorial plane, so that $\theta = \pi/2$, and we provide details of how $V(R)$ can be determined in Sec. IV of the Supplemental Material [33].

For a stable circular orbit at (areal) radius R_0 the effective potential $V_{\rm eff}(R)$ must take a minimum there, so that we have $V'(R_0) \equiv (dV/dR)_{R_0} = \ell^2/R_0^3$. Since $\ell = g_{\varphi\varphi}u^\varphi = R^2 d\varphi/d\tau$, the proper time τ_φ needed to complete one orbit, i.e., to advance from an angle φ_0 to $\varphi_0 + 2\pi$, is given by

$$\tau_\varphi = \frac{2\pi R_0^2}{\ell} = 2\pi\left(\frac{R_0}{V'(R_0)}\right)^{1/2}. \tag{4}$$

In the vicinity of a stable circular orbit we may approximate the effective potential as a parabola $V_{\rm eff}(R) \simeq V_{\rm eff}(R_0) + k\eta^2/2$, where $k \equiv V''_{\rm eff}(R_0) > 0$ and $\eta \equiv R - R_0$. Inserting these into (2) and taking a derivative with respect to proper time τ results in the harmonic-oscillator equation $\ddot{\eta} + k\eta = 0$ for η, where the double dot denotes a second derivative with respect to τ. Accordingly, the proper time τ_R needed to travel from the orbit's pericenter to the apcenter and back to the pericenter is given by

$$\tau_R = \frac{2\pi}{k^{1/2}} = 2\pi \left(\frac{R_0}{3V'(R_0) + R_0 V''(R_0)} \right)^{1/2}, \tag{5}$$

and the ratio between the two times τ_R and τ_φ is

$$\frac{\tau_R}{\tau_\varphi} = \left(\frac{V'(R_0)}{3V'(R_0) + R_0 V''(R_0)} \right)^{1/2}. \tag{6}$$

For a Newtonian point-mass potential $V(R) = pR^{-1}$, where p is a constant, we have $\tau_R = \tau_\varphi$, as expected for Kepler orbits. For a harmonic-oscillator potential $V(R) = pR^2$ we have $\tau_R = \tau_\varphi/2$, so that the orbit, which is centered at and symmetric about the origin, features two pericenters in each revolution. According to Bertrand's theorem, these two cases are the *only* potentials that lead to closed orbits.

While perturbations of the point-mass potential in the stellar exterior are familiar—yielding, for example, the relativistic perihelion advance of Mercury—we now focus on the stellar interior. Specifically, we show in Sec. IV.B of the Supplemental Material [33] that, in the vicinity of the center, the potential $V(R)$ can be written in the form

$$V(R) = V_0 + pR^2 + qR^4 + \mathcal{O}(R^6), \tag{7}$$

where V_0, p, and q are constants. Inserting (7) into (6) and assuming $qR_0^2 \ll p$ we find, to leading order,

$$\frac{\tau_R}{\tau_\varphi} \simeq \frac{1}{2} \left(1 - \frac{qR_0^2}{2p} \right). \tag{8}$$

As the black hole advances from one pericenter to the next, its positional angle φ therefore advances by

$$\Delta\varphi = \frac{d\varphi}{d\tau}\tau_R - \pi \simeq -\frac{\pi}{2}\frac{qR_0^2}{p} \tag{9}$$

beyond the angle π that would result in a closed orbit.

We refer the reader to Sec. IV of the Supplemental Material [33] where the constants p and q are evaluated in general relativity for nearly circular orbits. Here we present a more transparent Newtonian treatment in order to illustrate the key ingredients. In the vicinity of the stellar center we may approximate the density as $\rho(R) \simeq \rho_c + \rho^{(2)}R^2/2$, where $\rho_c^{(n)} \equiv (d^n\rho/dR^n)_{R=0}$. Integrating once we find the enclosed mass $M(R)$, and integrating again we obtain the potential

$$V_{\rm Newton}(R) \simeq V_0 + \frac{2\pi G}{3}\rho_c R^2 + \frac{\pi G}{10}\rho_c^{(2)} R^4. \tag{10}$$

Comparing with (7) we identify both p and q and compute

$$\Delta\varphi_{\rm Newton} \simeq -\frac{3\pi}{40}\frac{\rho_c^{(2)} R_0^2}{\rho_c}. \tag{11}$$

Evidently, the Newtonian pericenter advance is related to the degree of inhomogeneity, consistent with our discussion above.

We may evaluate the term $\rho_c^{(2)}$ in (11) using the Newtonian equations of hydrostatic equilibrium. For a polytropic EOS (1) we find

$$\rho_c^{(2)} = -\frac{4\pi}{3}\frac{G\rho_c^2}{a_c^2}, \tag{12}$$

where $a = (\Gamma P/\rho)^{1/2}$ is the (Newtonian) speed of sound. Finally we may use the central condensation $\delta \equiv \rho_c/\bar{\rho}$, where $\bar{\rho} = 3M_*/(4\pi R_*^3)$ is the average density, to rewrite the Newtonian pericenter advance as

$$\Delta\varphi_{\rm Newton} \simeq \frac{3\pi}{40}\frac{GM_*}{a_c^2 R_*}\left(\frac{R_0}{R_*}\right)^2 \delta. \tag{13}$$

For Newtonian polytropes δ depends on Γ only (see Table I for specific values). For smaller Γ, δ is larger and a_c^2 smaller [for a given compaction $GM_*/(c^2R_*)$]; we therefore see that the pericenter advance is larger for a softer EOSs (for a given value of R_0/R_*).

While the above analysis captures the leading-order Newtonian terms, we have found that the pericenter advance in the NSs considered here is dominated by relativistic terms. However, the pericenter advance's dependence on the EOS's stiffness is similar to that observed from the above Newtonian analysis even in the context of general relativity—namely, a softer EOS will lead to a more rapid precession of the orbit, and therefore to higher-frequency GW beats. This can be observed in Fig. 1 as well as in the Table I, where we list pericenter adnvances $\Delta\varphi$ for nearly circular orbits ($\ell_{\rm frac} = 0.99$) close to the center ($R_{\rm frac} = 0.05$) for a range of polytropic indices. We compare numerical results from the integration of the geodesic equation with analytical results from the perturbation of nearly circular orbits and find excellent agreement.

The range of polytropic exponents Γ listed in Table I roughly covers values adopted in piecewise-polytropic approximations for candidate nuclear EOSs (see Table III in [47]; note in particular the larger range of values for Γ_3, which governs the high-density core). The resulting values of $\Delta\varphi$ show significant variation, suggesting that a potential

TABLE I. Numerical and analytical data for polytropic stellar models and pericenter advances for nearly circular orbits close to the center of a stellar host with compaction $GM_*/(c^2R_*) = 1/6$. We list, for different values of $\Gamma = 1 + 1/n$, Newtonian values of the central condensation $\delta = \rho_c/\bar{\rho}$ (which depends on the Γ alone) and the Newtonian estimate $\Delta\varphi/(R_0/R_*)^2$, adopting numerical solutions to the Lane-Emden equation, together with $\Delta\varphi$ for $R_0/R_* = 0.05$. For the relativistic data we computed δ from solutions to the OV equations. Adopting $R_0/R_* = 0.05$ again we computed $\Delta\varphi_{\rm num}$ from numerical solutions to the geodesic equations, using $\ell_{\rm frac} = 0.99$ for nearly circular orbits, and $\Delta\varphi_{\rm ana}$ analytically as presented in the Supplemental Material [33]. We also list the number of GW wave cycles $\mathcal{N}_{\rm GW}$ completed during a beat cycle [see Eq. (15)], and, assuming a host star with mass $M_* = 1.4M_\odot$, the orbital time τ_φ as well as the precession time $\tau_{\rm prec}$. In the last two columns we provide the corresponding GW frequencies $f^{\rm GW}_{\rm orb} \simeq 2(u^t\tau_\varphi)^{-1}$ and $f^{\rm GW}_{\rm beat} \simeq (u^t\tau_{\rm prec})^{-1}$ as measured by a distant observer.

		Newton			GR							
Γ	n	δ	$\Delta\varphi/(R_0/R_*)^2$	$\Delta\varphi$	δ	$\Delta\varphi_{\rm num}$	$\Delta\varphi_{\rm ana}$	$\mathcal{N}_{\rm GW}$	τ_φ [ms]	$\tau_{\rm prec}$ [ms]	$f^{\rm GW}_{\rm orb}$ [kHz]	$f^{\rm GW}_{\rm beat}$ [Hz]
1.75	1.33	4.89	1.26	0.00315	7.46	0.0161	0.0162	194	0.194	18.9	5.56	28.7
2.0	1.0	3.29	0.775	0.00193	3.98	0.00841	0.00844	372	0.273	51.0	4.48	12.1
2.25	0.8	2.60	0.556	0.00139	2.94	0.00608	0.00612	513	0.321	82.4	4.01	7.81
2.5	0.67	2.23	0.432	0.00108	2.43	0.00494	0.00498	630	0.354	111	3.73	5.91
2.75	0.57	2.00	0.352	0.00088	2.14	0.00427	0.00430	731	0.379	138	3.54	4.85
3.0	0.5	1.84	0.298	0.00075	1.94	0.00382	0.00385	816	0.398	163	3.41	4.18
3.25	0.44	1.72	0.257	0.00064	1.80	0.00351	0.00353	890	0.414	184	3.31	3.72
∞	0	1	0	0	1	0.00164	0.00165	1904	0.553	527	2.62	1.38

observation of the resulting GW beats would provide a sensitive probe of the EOS.

From the pericenter advance $\Delta\phi$ we may also compute the precession frequency. Since we defined $\Delta\varphi$ as the (excess) advance from one pericenter to the next, and since, to leading order, orbits in the stellar interior feature two pericenters per orbit, the angular precession frequency measured locally is given by $\Omega_{\rm prec} = 2\Delta\varphi/\tau_\varphi$, where τ_φ is the orbital (proper) period. Related to the precession frequency is the (proper) precession period $\tau_{\rm prec}$ that it takes either of the two GW polarization amplitudes to go through one complete cycle, i.e., for the pericenter to advance by an angle π,[1]

$$\tau_{\rm prec} = \frac{\pi}{\Omega_{\rm prec}} = \frac{\pi}{2\Delta\varphi}\tau_\varphi. \tag{14}$$

The number of orbits completed during a precession period $\tau_{\rm prec}$ is therefore $\mathcal{N}_{\rm orbit} = \tau_{\rm prec}/\tau_\varphi = \pi/(2\Delta\varphi)$. Since, during one revolution, the GW signal completes two cycles, the number of such GW cycles completed as either GW polarization goes through a full beat cycle associated with the GW envelope is given by

$$\mathcal{N}_{\rm GW} = 2\mathcal{N}_{\rm orbit} = \frac{\pi}{\Delta\varphi}. \tag{15}$$

For the orbits in Fig. 1, for example, we found $\Delta\phi = 0.0255$, 0.0597, and 0.127 for $\Gamma = \infty$, 3, and 2, respectively, resulting in $\mathcal{N}_{\rm GW} = 123$, 52.6, and 24.8. In Table I we also provide data for $\mathcal{N}_{\rm GW}$, τ_φ, and $\tau_{\rm prec}$ for the nearly circular orbits considered there.

[1]In the bottom panel of Fig. 1, for example, $\tau_{\rm prec} \simeq 1000M_*$.

The above periods are proper times as measured by an observer comoving with the PBH. For the nearly circular orbits in Table I we may simply multiply these periods with u^t in order to obtain the corresponding coordinate time periods. In Table I we list the resulting GW frequency associated with a single orbit, $f^{\rm GW}_{\rm orb} \simeq 2/(u^t\tau_\varphi)$, and the GW beat frequency $f^{\rm GW}_{\rm beat} \simeq 1/(u^t\tau_{\rm prec})$, both as measured by a distant observer.

To summarize, we discuss quasiperiodic GW beats as a qualitatively new feature of continuous GW signals emitted by PBHs captured inside NSs. The beats are due to orbital precession, which is caused both by relativistic effects and density nonuniformity. Adopting a polytropic EOS we demonstrate both numerically and analytically that the beat frequency depends quite strongly on the structure of the NS and hence the stiffness of the EOS. For the NSs considered here the precession rate and beat frequency are largely due to relativistic gravitation, so that a Newtonian treatment would significantly underestimate the effect. If such beats were to be observed by next-generation GW detectors, e.g., the Einstein Telescope [48], the Cosmic Explorer [49], or the Neutron Star Extreme Matter Observatory (NEMO) [50], they would therefore provide valuable constraints on the nuclear EOS.

Clearly, the beat frequency also depends on the radius and eccentricity of the PBH's orbit, which would have to be found independently. The latter is related to the relative maximum and minimum amplitudes in each one of the GW polarizations, and it may be possible to determine the radius from the prior inspiral signal. Knowing these orbital parameters, as well as the host star's compaction, an observed beat frequency could then be compared with those found for orbits inside general relativistic stellar models constructed for

candidate nuclear EOSs. While the GW amplitude depends on the PBH mass, the precession frequency does not.

We would like to thank Steve Naculich, David Kaiser, and Keith Riles for helpful conversations. T. W. B. gratefully acknowledges the hospitality of the University of Arizona's Steward Observatory. This work was supported in part by National Science Foundation (NSF) Grants No. PHY-2010394 and No. PHY-2341984 to Bowdoin College, as well as NSF Grants No. PHY-2006066 and No. PHY-2308242 to the University of Illinois at Urbana-Champaign.

[1] Y. B. Zel'dovich and I. D. Novikov, The hypothesis of cores retarded during expansion and the hot cosmological model, Sov. Astron. **10**, 602 (1967).
[2] S. W. Hawking, Gravitationally collapsed objects of very low mass, Mon. Not. R. Astron. Soc. **152**, 75 (1971).
[3] B. J. Carr and S. W. Hawking, Black holes in the early universe, Mon. Not. R. Astron. Soc. **168**, 399 (1974).
[4] M. Y. Khlopov, Primordial black holes, Res. Astron. Astrophys. **10**, 495 (2010).
[5] B. Carr and F. Kühnel, Primordial black holes as dark matter: Recent developments, Annu. Rev. Nucl. Part. Sci. **70**, 355 (2020).
[6] B. Carr, K. Kohri, Y. Sendouda, and J. Yokoyama, Constraints on primordial black holes, Rep. Prog. Phys. **84**, 116902 (2021).
[7] A. A. Jackson and M. P. Ryan, Was the Tungus event due to a black hole?, Nature (London) **245**, 88 (1973).
[8] W. H. Beasley and B. A. Tinsley, Tungus event was not caused by a black hole, Nature (London) **250**, 555 (1974).
[9] G. M. Fuller, A. Kusenko, and V. Takhistov, Primordial black holes and *r*-process nucleosynthesis, Phys. Rev. Lett. **119**, 061101 (2017).
[10] J. Bramante, T. Linden, and Y.-D. Tsai, Searching for dark matter with neutron star mergers and quiet kilonovae, Phys. Rev. D **97**, 055016 (2018).
[11] M. A. Abramowicz, M. Bejger, and M. Wielgus, Collisions of neutron stars with primordial black holes as fast radio bursts engines, Astrophys. J. **868**, 17 (2018).
[12] D. W. P. Amaral and E. D. Schiappacasse, Rescuing the primordial black holes all-dark matter hypothesis from the fast radio bursts tension, arXiv:2312.09285.
[13] V. Takhistov, Transmuted gravity wave signals from primordial black holes, Phys. Lett. B **782**, 77 (2018).
[14] V. Takhistov, G. M. Fuller, and A. Kusenko, Test for the origin of solar mass black holes, Phys. Rev. Lett. **126**, 071101 (2021).
[15] M. Abramowicz, M. Bejger, A. Udalski, and M. Wielgus, A robust argument on the existence of primordial black holes in galactic dark matter halos, Astrophys. J. Lett. **935**, L28 (2022).
[16] M. Oncins, J. Miralda-Escudé, J. L. Gutiérrez, and P. Gil-Pons, Primordial black holes capture by stars and induced collapse to low-mass stellar black holes, Mon. Not. R. Astron. Soc. **517**, 28 (2022).
[17] V. Takhistov, Positrons from primordial black hole microquasars and gamma-ray bursts, Phys. Lett. B **789**, 538 (2019).
[18] C. Bambi, D. Spolyar, A. D. Dolgov, K. Freese, and M. Volonteri, Implications of primordial black holes on the first stars and the origin of the super-massive black holes, Mon. Not. R. Astron. Soc. **399**, 1347 (2009).
[19] K. M. Belotsky, A. E. Dmitriev, E. A. Esipova, V. A. Gani, A. V. Grobov, M. Y. Khlopov, A. A. Kirillov, S. G. Rubin, and I. V. Svadkovsky, Signatures of primordial black hole dark matter, Mod. Phys. Lett. A **29**, 1440005 (2014).
[20] K. M. Belotsky, V. I. Dokuchaev, Y. N. Eroshenko, E. A. Esipova, M. Y. Khlopov, L. A. Khromykh, A. A. Kirillov, V. V. Nikulin, S. G. Rubin, and I. V. Svadkovsky, Clusters of primordial black holes, Eur. Phys. J. C **79**, 246 (2019).
[21] E. Bagui, S. Clesse, V. De Luca, J. María Ezquiaga, G. Franciolini, J. García-Bellido, C. Joana, R. K. Jain, S. Kuroyanagi, I. Musco, T. Papanikolaou, A. Raccanelli, S. Renaux-Petel, A. Riotto, E. Ruiz Morales, M. Scalisi, O. Sergijenko, C. Unal, V. Vennin, and D. Wands, Primordial black holes and their gravitational-wave signatures, arXiv:2310.19857.
[22] B. Bertrand, M. Cuadrat-Grzybowski, P. Defraigne, M. Van Camp, and S. Clesse, Observing dark matter clumps and asteroid-mass primordial black holes in the solar system with gravimeters and GNSS networks, arXiv:2312.14520.
[23] T. X. Tran, S. R. Geller, B. V. Lehmann, and D. I. Kaiser, Close encounters of the primordial kind: A new observable for primordial black holes as dark matter, arXiv:2312.17217.
[24] F. Capela, M. Pshirkov, and P. Tinyakov, Constraints on primordial black holes as dark matter candidates from capture by neutron stars, Phys. Rev. D **87**, 123524 (2013).
[25] P. Montero-Camacho, X. Fang, G. Vasquez, M. Silva, and C. M. Hirata, Revisiting constraints on asteroid-mass primordial black holes as dark matter candidates, J. Cosmol. Astropart. Phys. 08 (2019) 031.
[26] Y. Génolini, P. D. Serpico, and P. Tinyakov, Revisiting primordial black hole capture into neutron stars, Phys. Rev. D **102**, 083004 (2020).
[27] W. E. East and L. Lehner, Fate of a neutron star with an endoparasitic black hole and implications for dark matter, Phys. Rev. D **100**, 124026 (2019).
[28] C. B. Richards, T. W. Baumgarte, and S. L. Shapiro, Accretion onto a small black hole at the center of a neutron star, Phys. Rev. D **103**, 104009 (2021).
[29] S. C. Schnauck, T. W. Baumgarte, and S. L. Shapiro, Accretion onto black holes inside neutron stars with piecewise-polytropic equations of state: Analytic and numerical treatments, Phys. Rev. D **104**, 123021 (2021).

[30] M. A. Abramowicz, J. K. Becker, P. L. Biermann, A. Garzilli, F. Johansson, and L. Qian, No observational constraints from hypothetical collisions of hypothetical dark halo primordial black holes with galactic objects, Astrophys. J. **705**, 659 (2009).
[31] C. J. Horowitz and S. Reddy, Gravitational waves from compact dark objects in neutron stars, Phys. Rev. Lett. **122**, 071102 (2019).
[32] Z.-C. Zou and Y.-F. Huang, Gravitational-wave emission from a primordial black hole inspiraling inside a compact star: A novel probe for dense matter equation of state, Astrophys. J. Lett. **928**, L13 (2022).
[33] See Supplemental Material at http://link.aps.org/supplemental/10.1103/PhysRevD.110.L021303 for an estimate of event rates, the construction of stellar background models, the equations of motion, as well as a perturbative analysis of nearly circular orbits.
[34] I. Goldman and S. Nussinov, Weakly interacting massive particles and neutron stars, Phys. Rev. D **40**, 3221 (1989).
[35] S. D. McDermott, H.-B. Yu, and K. M. Zurek, Constraints on scalar asymmetric dark matter from black hole formation in neutron stars, Phys. Rev. D **85**, 023519 (2012).
[36] P. Pani and A. Loeb, Tidal capture of a primordial black hole by a neutron star: Implications for constraints on dark matter, J. Cosmol. Astropart. Phys. 06 (2014) 026.
[37] Q. Gao, N. Dai, Y. Gong, C. Zhang, C. Zhang, and Y. Zhao, Probe the equation of state for neutron stars with captured primordial black holes inside, arXiv:2306.06645.
[38] J. B. Hoffer, The effect of dynamical friction on orbits—The case of a particle orbiting a central point mass embedded in a massless stellar system, Astrophys. J. **289**, 193 (1985).
[39] Á. Szölgyén, M. MacLeod, and A. Loeb, Eccentricity evolution in gaseous dynamical friction, Mon. Not. R. Astron. Soc. **513**, 5465 (2022).
[40] T. W. Baumgarte and S. L. Shapiro, Primordial black holes captured by neutron stars: Relativistic point-mass treatment, Phys. Rev. D **109**, 123012 (2024).
[41] Animation, an animation of Fig. 1 can be found at https://youtu.be/0cyupaob7L4.
[42] P. C. Peters and J. Mathews, Gravitational radiation from point masses in a Keplerian orbit, Phys. Rev. **131**, 435 (1963).
[43] P. C. Peters, Gravitational radiation and the motion of two point masses, Phys. Rev. **136**, B1224 (1964).
[44] C. W. Misner, K. S. Thorne, and J. A. Wheeler, *Gravitation* (Freeman, San Francisco, 1973).
[45] J. L. F. Bertrand, Théorème relatif au mouvement d'un point attiré vers un centre fixe, C.R. Acad. Sci. Paris **77**, 849 (1873).
[46] H. Goldstein, *Classical Mechanics* (Addison-Wesley, New York, 1980).
[47] J. S. Read, B. D. Lackey, B. J. Owen, and J. L. Friedman, Constraints on a phenomenologically parametrized neutron-star equation of state, Phys. Rev. D **79**, 124032 (2009).
[48] The Einstein Telescope, https://www.et-gw.eu.
[49] The Cosmic Explorer, https://cosmicexplorer.org.
[50] K. Ackley *et al.*, Neutron star extreme matter observatory: A kilohertz-band gravitational-wave detector in the global network, Pub. Astron. Soc. Aust. **37**, e047 (2020).